IEEE Access
Multidisciplinary | Rapid Review | Open Access Journal

Received August 29, 2019, accepted October 5, 2019, date of publication October 9, 2019, date of current version October 23, 2019.

Digital Object Identifier 10.1109/ACCESS.2019.2946518

Energy-Saving Nonlinear Friction Compensation Method for Direct Drive Volume Control Flange-Type Rotary Vane Steering Gear

L. H. LIANG, L. Y. WANG, AND J. F. WANG
College of Automation, Harbin Engineering University, Harbin 150001, China
Corresponding author: L. Y. Wang (luyangwang1987@foxmail.com)

ABSTRACT In the research of various energy technologies, the direct-drive volume control flange-type rotary vane steering gear (DDVC–FRVSG) has become a promising component for controlling the course and posture of a vessel because of its superior energy-saving performance. However, nonlinear friction limits the ability of the DDVC–FRVSG to satisfy the efficient energy requirements of the vessel. This study proposes compensation methods to suppress nonlinear friction, such that the rudder can be efficiently controlled. Based on the principle of the DDVC–FRVSG, we establish a mathematical model and transfer function of the steering gear system along with a mathematical model of the impact of nonlinear friction on the rudder system. A friction model-based method using the integral back-stepping adaptive control strategy is proposed to suppress nonlinear friction, and both the models are studied theoretically and through simulation. Taking the no-compensation state as a benchmark, our measured results by prototype testing reveal that the method can compensate for nonlinear friction, achieving up to 73.08 % better performance on average and reducing the output power of the driving motor by 36.39 % on average. The findings of this research will contribute to the energy-saving performance and efficient energy requirement of the DDVC–FRVSG system.

INDEX TERMS DDVC–FRVSG, energy-saving, friction compensation.

I. INTRODUCTION

The total amount of energy carried by ships is fixed. Therefore, the energy consumption in ship motion control must be reduced as much as possible to ensure ship endurance [1]. In addition to the traditional course control function under low-frequency working status, ship rudder also poses increasing demands for the rudder roll stabilization under high-frequency working status [2], [3]. In the process of overcoming the interference effects of unnecessary energy consumption by various nonlinear factors, energy cannot achieve the highest efficiency. However, the increasing demands of high efficiency and energy saving establish a higher requirement for dynamic performance, such as rudder response speed and frequency response [4]. Therefore, designing appropriate control strategies to overcome nonlinear factors influencing the dynamic performance of the steering gear and realizing a more efficient use of steering gear energy have become important research directions.

The associate editor coordinating the review of this manuscript and approving it for publication was Haiyong Zheng.

The direct-drive volume control flange-type rotary vane steering gear (DDVC–FRVSG), which combines the ''DDVC system'' with a ''rotary rudder of flange-type structure,'' is a type of electro-hydraulic servo steering gear that integrates all the advantages of the DDVC drive mechanism and the rotary vane rudder of the flange-type structure [5]. Fig. 1 shows a schematic of the considered system. The nonlinearity of the DDVC–FRVSG system is derived from its operating environment (i.e., the nonlinearity of the external load moments applied on the rudder) [6]. The hydrodynamic moment, friction torque, and inertia moment exerted on the DDVC–FRVSG system in the form of external load enable nonlinear feature in its dynamic performance [8]–[10]. Among the external loading moment borne by the system, the friction torque makes the system unable to track the instruction of rudder angle quickly and accurately, and the nonlinearity resulting therefrom has a larger influence on the dynamic performance of the rudder. Moreover, it will generate unnecessary energy consumption during such a process [11]. Therefore, an in-depth study of the friction characteristics of DDVC–FRVSG and its compensation strategy is of

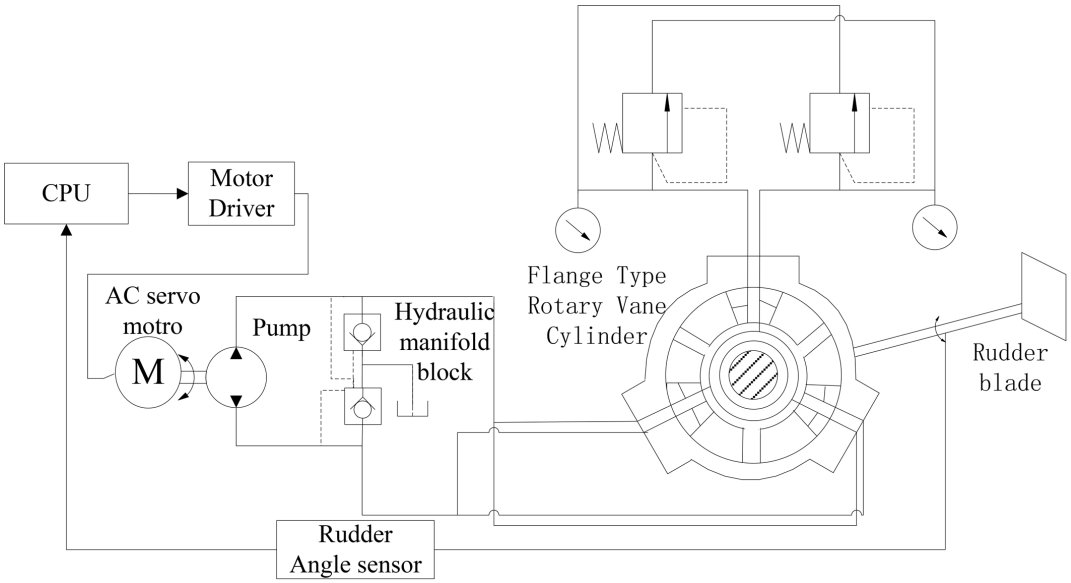

FIGURE 1. Schematic of the DDVC–FRVSG.

great significance to the improvement of the efficiency of the steering gear and the saving of marine energy [16]. Among various friction models [19], the LuGre model provides the most complete information and can accurately describe the static and dynamic performances of friction. Thus, the compensation method is usually based on the LuGre model [22]. Considering that friction exists in the relative motion process for almost every mechanical system [12], many methods for friction compensation have been attempted in different types of servo control systems [22]. Through experimental studies, Canadus de Wit et al. analyzed the impact of load-type change on the friction model and designed an adaptive regulating controller for the model [20], [21], thus putting forward a bristle model to identify the parameters of the motor servo control system. With regard to Bosch GPA-S electro-mechanical actuator [23], Kebairi et al. put forward a series of friction modeling and identification methods. On the basis of a cascaded structure, Luc Le-Tien and Alin Albu-Schaffer put forward a robust adaptive control scheme flexible-joint robots taking a full state feedback controller with integrator terms such as inner control loop, and the computed torque as outer control loop. Their research, which was conducted based on the LuGre friction model, designed an adaptive friction compensation, and adopted the joint torque feedback in the state feedback controller to dampen the structural oscillations of the link side effectively [24]. A simplified adaptive command-filtered back-stepping control (CFBC) framework for robotic arms, which was driven by a series elastic actuator (SEA), was put forward by Yongping Pan et al. For this, an adaptive mechanism was adopted to compensate for the discontinuous friction, thereby alleviating the complexity problem in integrator back-stepping control. It has attracted considerable attention [25]. Sergey Edward Lyshevski, who examined nonlinear mechatronic systems with direct-drive limited-angle axial-topology actuators, used the estimated parameters to design the tracking control laws that compensate friction. A nonlinear feedback can be used to compensate the adverse friction, ensuring the adaptive reconfiguration by estimating the unknown parameters in near real-time [26]. Liu N et al. adopted the back-stepping method and proposed an attitude-restricted dynamic surface (DSC) controller [27]. K. A. J. Verbert et al., through simulation and in the real world, presented an adaptive friction compensation scheme and confirmed that the compensator, which can eliminate steady-state errors and decrease the stick-slip effect significantly, can compensate even with rapidly varying friction forces [28]. In view of the nonlinearity, modeling uncertainty, severe measurement noise arising from the actual state feedback, and deteriorating control performance, JY Yao et al. presented a desired compensation adaptive controller to control the motion of electro-hydraulic servo systems precisely. As revealed by the theoretical analysis and experimental results, even under parametric uncertainties and uncertain nonlinearities, the proposed controller can guarantee a prescribed transient performance and final tracking accuracy [29]. Zhang et al. put forward a Lyapunov-theory-based compensation method, which uses the LuGre model to identify the parameters of the friction model online, to compensate for the nonlinear friction when the ball-screw electro-mechanical servo system operates. Moreover, they adopted an integral back-stepping adaptive control method to design a compensation controller, using which ideal compensation effects were obtained [30]–[43].

Analogous to the ball-screw electro-mechanical servo system, this paper proposes an integral back-stepping adaptive control strategy for friction compensation of the DDVC–FRVSG system to improve its dynamic performance and thus reduce its energy consumption during the operation

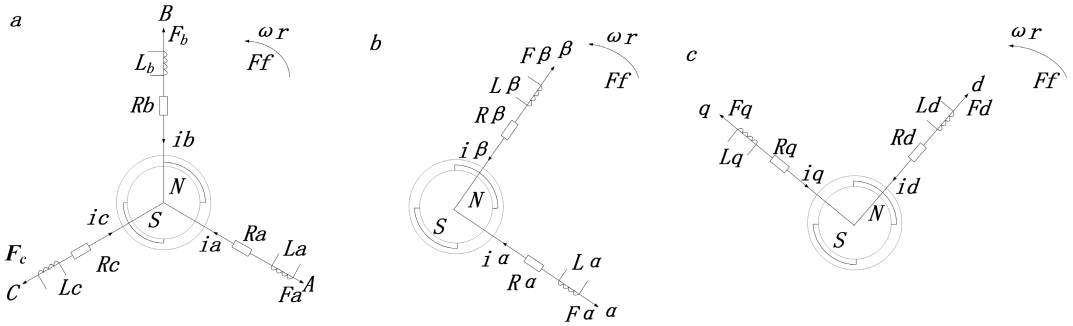

FIGURE 2. PMSM under the three-phase stator coordinate system.

of the steering gear. First, the mathematical model of the DDVC–FRVSG system is established. Then, the friction phenomenon of the system is described based on the LuGre model. Then, the integral back-stepping adaptive control strategy is applied to the system to compensate the friction phenomenon. Through the joint simulation of AMESim/Simulink, the improvement of dynamic performance and the increase and decrease of energy consumption before and after compensation, respectively, are observed. Regardless of the hydrodynamic action, this study describes the system's dynamic performance as a simulate curve of the rudder angle response and describes the system's efficiency and energy-saving performance as a simulate curve of motor power. All results were verified through simulations. The integral back-stepping adaptive control strategy can effectively compensate the friction phenomenon of the DDVC–FRVSG system to improve the dynamic performance of the system and effectively reduce the energy consumption of the system.

II. STRUCTURE AND PRINCIPLE OF THE DDVC–FRVSG

A. SYSTEM DESCRIPTION

The DDVC–FRVSG system is an electro-hydraulic system. The fixed displacement pump and the flange-type rotary vane steering gear are connected with hydraulic pipes, forming a closed hydraulic circuit. At the other end of the pump, an AC servo-motor drives the pump rotation through the controller to supply oil to the flange-type rotary vane steering gear, driving the rudder rotation. The rotary speed of the rudder is controlled by the AC servomotor, and the direction is changed via motor shaft rotation. Therefore, an angle sensor is used in a closed-loop feedback to achieve control of the rotation of the steering gear.

B. SYSTEM MODELING

The system input is the order rotary speed of the servomotor, and its output is the shaft angle of the rudder. The objective is to design a model that accurately describes the relationship between the order rotary speed of the servomotor and the output of the shaft angle.

1) MATHEMATICAL MODEL OF SERVO MOTOR

The motor used in this system is an AC permanent magnet synchronous motor (PMSM), which can realize vector control through coordinate transformation during control. The specific transformation principle can be described as follow. The stator current (AC) i_A, i_B, and i_C of the AC motor under the three-phase stationary coordinate system is equivalent to AC current i_α and i_β through transformation from three phases to two phases. i_α and i_β obtained is equivalent to current i_d and i_q under the synchronous rotation coordinate system through transformation from two-phase stationary coordinate system to two-phase rotating coordinate system. Based on the aforesaid coordinate transformation principle, the mathematical model of the PMSM is described as follows: Based on the analytical model of the PMSM under the three-phase stator coordinate system shown in Figure 2, the voltage equation of the PMSM under such a coordinate system is shown as (1).

$$\begin{bmatrix} u_A \\ u_B \\ u_C \end{bmatrix} = \begin{bmatrix} R_s + Lp & 0 & 0 \\ 0 & R_s + Lp & 0 \\ 0 & 0 & R_s + Lp \end{bmatrix} \begin{bmatrix} i_A \\ i_B \\ i_C \end{bmatrix} - \omega_r \psi_f \begin{bmatrix} \sin\theta_m \\ \sin\left(\theta_m - \frac{2}{3}\pi\right) \\ \sin\left(\theta_m + \frac{2}{3}\pi\right) \end{bmatrix} \tag{1}$$

As shown in the analytical model under the two-phase stationary coordinate system indicated in Figure 2, whereas α axis overlaps with A axis and β axis is 90 ahead of α axis in the direction of rotor rotation. During coordinate transformation, the power of the motor is usually unchanged before and after transformation. Assuming that the number of turns in each phase of the three-phase (two-phase) stator winding is N_3 (N_2), and the three-phase(two-phase) stator synthetic magneto motive force is F_{3s}(F_{2s}), based on (3) and (4), assuming $F_{3s} = F_{2s}$ and $N_3/N_2 = \sqrt{2/3}$, by the (5) obtained, it can finally obtain the current transition matrix through transformation from three phases to two phases as shown in (5).

$$F_{3s} = N_3\left(i_A + i_B e^{j\frac{2}{3}\pi} + i_C e^{j\frac{4}{3}\pi}\right) \tag{2}$$

$$F_{2s} = N_2\left(i_\alpha + i_\beta e^{j\frac{\pi}{2}}\right) \tag{3}$$

$$\left(i_\alpha + i_\beta e^{j\frac{2}{3}\pi}\right) = \frac{N_3}{N_2}\left(i_A + i_B e^{j\frac{2}{3}\pi} + i_C e^{j\frac{4}{3}\pi}\right) \tag{4}$$

$$\begin{bmatrix} i_\alpha \\ i_\beta \end{bmatrix} = \sqrt{\frac{2}{3}}\begin{bmatrix} 1 & -\frac{1}{2} & -\frac{1}{2} \\ 0 & \frac{\sqrt{3}}{2} & -\frac{\sqrt{3}}{2} \end{bmatrix}\begin{bmatrix} i_A \\ i_B \\ i_C \end{bmatrix} = T\begin{bmatrix} i_A \\ i_B \\ i_C \end{bmatrix} \tag{5}$$

Based on the principle of the consistent transformation of the magneto motive force, the voltage and current in the mathematical model of the motor, the loop voltage equation under the two-phase stationary coordinate system can be obtained, as shown in (6).

$$\begin{bmatrix} u_\alpha \\ u_\beta \end{bmatrix} = \begin{bmatrix} R_s + L_\alpha p & 0 \\ 0 & R_s + L_\beta p \end{bmatrix} T \begin{bmatrix} i_A \\ i_B \\ i_C \end{bmatrix} + \sqrt{\frac{3}{2}}\omega_r \psi_f \begin{bmatrix} -\sin\theta_m \\ \cos\theta_m \end{bmatrix} \tag{6}$$

The torque equation is given by (7).

$$T_n = i_\beta\sqrt{\frac{3}{2}}\psi_f \cos\theta_m - i_\alpha\sqrt{\frac{3}{2}}\psi_f \sin\theta_m \tag{7}$$

On the other hand, $R_\alpha = R_\beta = R_s, L_\alpha = L_\beta = 1.5L$.

It can be known from the analytical model shown in Figure 2c that under the two-phase rotating coordinate system, the d axis overlaps with the direction of flux-linking ψ_f generated by the rotor. In such cases, the angle between the d axis and α axis is θ_m, based on the principle that the magneto motive force remains unchanged before and after transformation, assuming that N_2' denotes the equivalent number of turns for each phase of the winding under the d-q coordinate system. Then, the current transformation is shown as (8).

$$\begin{bmatrix} i_d \\ i_q \end{bmatrix} = \frac{N_2}{N_2'}\begin{bmatrix} \cos\theta_m & \sin\theta_m \\ -\sin\theta_m & \cos\theta_m \end{bmatrix}\begin{bmatrix} i_\alpha \\ i_\beta \end{bmatrix} \tag{8}$$

Based on the condition that the power remains unchanged before and after transformation, we assume $N_2/N_2' = 1$. Based on the aforementioned analysis, the voltage of the d-q axis is given by (9).

$$\begin{bmatrix} u_d \\ u_q \end{bmatrix} = \begin{bmatrix} R_s & 0 \\ 0 & R_s \end{bmatrix}\begin{bmatrix} i_d \\ i_q \end{bmatrix} + \begin{bmatrix} p & -\omega \\ \omega & p \end{bmatrix}\begin{bmatrix} \psi_d \\ \psi_q \end{bmatrix} \tag{9}$$

As the q axis is orthogonal with ψ_f, the component of rotor flux-linking on the q axis is 0. Using n_p to indicate the pole pairs of the motor, the flux-linking equation and torque equation is given by (10) and (11), respectively:

$$\begin{bmatrix} \psi_d \\ \psi_q \end{bmatrix} = \begin{bmatrix} L_d & 0 \\ 0 & L_q \end{bmatrix}\begin{bmatrix} i_d \\ i_q \end{bmatrix} + \begin{bmatrix} \psi_f \\ 0 \end{bmatrix} \tag{10}$$

$$T_e = n_p\left[\psi_f i_q + \left(L_d - L_q\right) i_d i_q\right] \tag{11}$$

Then, the equation of motion for the PMSM is given by (12)

$$T_n - T_{load} = \frac{1}{n_p}J_T\ddot{\theta}_m + \frac{1}{n_p}D\dot{\theta}_m \tag{12}$$

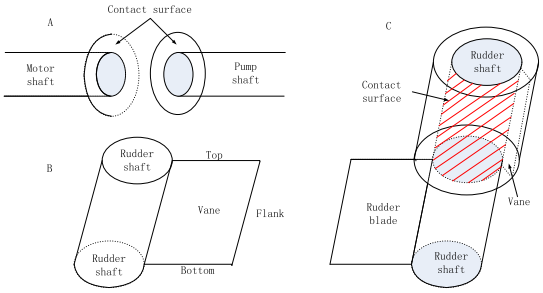

FIGURE 3. The surface that exhibits friction.

2) MATHEMATICAL MODEL OF HYDRAULIC PART

It can be known from [44] that the mathematical model of the hydraulic part of the system can be established by (13)−(15).

$$Q_L = nD_p = \dot{\theta}_m D_p \tag{13}$$

$$nD_p - C_{ip}(p_1 - p_2) - C_{ep}p_1 - C_{im}(p_1 - p_2) - C_{em}p_1 = D_m\frac{d\theta}{dt} + \frac{V_t}{4\beta_e}\frac{dp_1}{dt} + \left(C_{im} + \frac{1}{2}C_{em}\right)p_1 \tag{14}$$

$$T_g = (p_1 - p_2)D_m = J_m\frac{d^2\theta}{dt^2} + B_m\frac{d\theta}{dt} + G\theta + T_{friction} + T_L \tag{15}$$

3) TRANSFER FUNCTION OF SYSTEM

The transfer function of the DDVC–FRVSG system can be established using (16)

$$\begin{aligned} G_p(s) &= \frac{\theta(s)}{N(s)} = \frac{4\beta_e D_m D_p}{V_t J_m s^3 + V_t B_m s^2 + 4\beta_e D_m^2 s} \\ &= \frac{4\beta_e D_m D_p}{s(V_t J_m s^2 + V_t B_m s + 4\beta_e D_m^2)} \\ &= \frac{\frac{D_p}{D_m}}{s(\frac{s^2}{\omega_h^2} + \frac{2\xi_h}{\omega_h}s + 1)} \end{aligned} \tag{16}$$

C. NOMENCLATURE

Table 1 lists the nomenclature of this paper.

III. FRICTION AND ITS EFFECT ON THE SYSTEM

It can be known from [44] that the existence of friction torque in the DDVC–FRVSG system and the system LuGre friction model with two dynamic coefficients and four static coefficients are shown in (17)−(23). Fig. 3 shows the surface that exhibits friction.

$$T_{friction} = T_{friction1} + T_{friction2} + T_{friction3} + T_{friction4} \tag{17}$$

$$\begin{cases} T_{friction1} = \sigma_{0m}z_m + \sigma_{1m}\dot{z_m} + B_{\theta_m}\dot{\theta_m} \\ \dot{z_m} = \dot{\theta_m} - \dfrac{|\dot{\theta_m}|}{g(\dot{\theta_m})}z_m \\ \sigma_{0m}g(\dot{\theta_m}) = T_{cm} + (T_{sm} - T_{cm})\,e^{-[\frac{\dot{\theta_m}}{\dot{\theta_m}}]^2} \end{cases} \tag{18}$$

$T_{friction2}$

TABLE 1. Units for magnetic properties.

Symbol	Quantity	Unite
D_p	Displacement of pump	m^3/rev
n	Rotary speed of pump	rev/s
D_m	Radian displacement	m^3/rad
β_e	Volumetric modulus of elasticity	Pa
θ	Angle of rudder	rad
V_p	Volume of high-pressure chamber of the pump	m^3
V_g	Volume of pipes	m^3
C_ip	Pump coefficient of internal leakage	m^3/Pa
C_ep	Pump coefficient of external leakage	m^3/Pa
C_im	Rotary vane cylinder coefficient of internal leakage	m^3/Pa
C_em	Rotary vane cylinder coefficient of external leakage	m^3/Pa
p_1	Pressure of high-pressure chamber	Pa
p_2	Pressure of low-pressure chamber	Pa
T_g	Torque of rotary vane steering gear	$N \cdot m$
J_m	Total rotary inertia residual to the cylinder and load	$kg \cdot m^2$
B_m	Viscous damping coefficient	$N \cdot m/(rad/s)$
G	Loading spring stiffness	$N \cdot m/rad$
$T_{friction}$	Friction torque of the steering gear	$N \cdot m$
T_L	External torque beside friction	$N \cdot m$
D	Damping coefficient of the motor shaft	$N \cdot m/(rad/s)$
J_T	Rotary inertia residual of the motor shaft	$kg \cdot m^2$
T_n	Electromagnetic torque of the motor	$N \cdot m$
θ_m	Output location of the motor shaft	rad
U	Control voltage of the motor driver	V
k_{ac}	Proportionality coefficient of control voltage	zero dimension
R_a	Stator resistance	Ω
$u_{A,B,C}$	Stator voltage of three-phase stationary coordinate system	V
$i_{A,B,C}$	Stator current of three-phase stationary coordinate system	A
$u_{\alpha,\beta}$	Stator voltage of two-phase stationary coordinate system	V
$i_{\alpha,\beta}$	Stator current of two-phase stationary coordinate system	A
$u_{d,q}$	Stator voltage of two-phase rotating coordinate system	V
$i_{d,q}$	Stator current of two-phase rotating coordinate system	A
L	Auto conduction	L
ψ_f	Permanent magnet flux linkage	Wb
$N_{2,3}$	Number of stator winding turns	zero dimension
$F_{2s,3s}$	Synthesis MMF	At
T_{load}	Loading torque of the motor	$N \cdot m$
ω_h	Inherent frequency of the system	rad/s
ξ_h	Damping ratio of the system	zero dimension
σ_{0n}	Bristle rigidity coefficient	Nm/s
σ_{1n}	Bristle damping coefficient	N/m
T_{cm}	Coulomb friction torque	Nm
T_{sm}	Static friction torque	Nm
F_{cn}	Coulomb friction force	N
F_{sn}	Static friction force	N
$B_{\theta n}$	Viscous friction coefficient	Nm/s
R	Radius of the vane	m
r	Radius of each point on the surface of top and bottom	m
R_r	Radius of the rudder shaft	m
$r\theta_s$,$R\theta_s$,$R_r\theta_s$	Stribeck speed	rad/s

$$= T_{frictionUP} + T_{frictionDOWN} + T_{frictionFLANK} \tag{19}$$

$$\begin{cases} F_{fUP} = F_{fDOWN} = \int_0^R [\sigma_0 z + \sigma_1 \dot{z} + B_{\theta 2}(\dot{r\theta})]dr \\ F_{fFLANK} = \sigma_0 z + \sigma_1 \dot{z} + B_{\theta 2}(\dot{R\theta}) \end{cases} \tag{20}$$

$$\begin{cases} T_{friction2} = 2\int_0^R r[\sigma_{01} z_1 + \sigma_{11}\dot{z_1} + B_{\theta 2}(\dot{r\theta})]dr \\ +R[\sigma_{02} z_2 + \sigma_{12}\dot{z_2} + B_{\theta 2}(\dot{R\theta})] \\ \dot{z_1} = \dot{r\theta} - \dfrac{|(\dot{r\theta})|}{g(\dot{r\theta})} z_1,\ \dot{z_2} = \dot{R\theta} - \dfrac{|(\dot{R\theta})|}{g(\dot{R\theta})} z_2 \\ \sigma_{01} g(\dot{r\theta}) = F_{c1} + (F_{s1} - F_{c1})\, e^{-[\frac{\dot{r\theta}}{(\dot{r\theta})_s}]^2} \\ \sigma_{02} g(\dot{R\theta}) = F_{c2} + (F_{s2} - F_{c2})\, e^{-[\frac{\dot{R\theta}}{(\dot{R\theta})_s}]^2} \end{cases} \tag{21}$$

$$\begin{cases} T_{friction3} = R_r[\sigma_{03} z_3 + \sigma_{13}\dot{z_3} + B_{\theta 3}(\dot{R_r\theta})] \\ \dot{z_3} = (\dot{R_r\theta}) - \dfrac{|(\dot{R_r\theta})|}{g(\dot{R_r\theta})} z_3 \\ \sigma_{03} g(\dot{R_r\theta}) = F_{c3} + (F_{s3} - F_{c3})\, e^{-[\frac{(\dot{R_r\theta})}{(\dot{R_r\theta})_s}]^2} \end{cases} \tag{22}$$

$$\begin{aligned} T_{ss} &= T_{cm} + (T_{sm} - T_{cm})\, e^{-[\frac{\dot{\theta_m}}{(\dot{\theta_m})_s}]^2} sgn(\dot{\theta_m}) + B_{\theta m}(\dot{\theta_m}) \\ &+2r[F_{c1} + (F_{s1} - F_{c1})\, e^{-[\frac{(\dot{r\theta})}{(\dot{r\theta})_s}]^2} sgn((\dot{r\theta})) + B_{\theta 1}((\dot{r\theta}))] \\ &+R[F_{c2} + (F_{s2} - F_{c2})\, e^{-[\frac{(\dot{R\theta})}{(\dot{R\theta})_s}]^2} sgn((\dot{R\theta})) + B_{\theta 2}((\dot{R\theta}))] \\ &+R_r[F_{c3} + (F_{s3} - F_{c3})\, e^{-[\frac{(\dot{R_r\theta})}{(\dot{R_r\theta})}]^2} sgn((\dot{R_r\theta})) \\ &+B_{\theta 3}((\dot{R_r\theta}))] \end{aligned} \tag{23}$$

IV. COMPENSATION METHOD

This section discusses further research on the compensation method of friction torque in the working process of the DDVC–FRVSG system.

As mentioned in the references, based on characteristics of friction, the DDVC–FRVSG system adopts the compensation methods based on a model. The real substance of the compensation, based on the model, is a feed-forward compensation process. The process is built upon the mathematical model of friction to describe and identify the relevant system parameters (e.g., value and direction of friction torque) according to the loading running speed, displacement, and other parameters. Next, the controller exerts the same torque in the opposite direction to the system to suppress the friction interference and eliminate the friction effects.

The system model is given by (16); T_n is approximately equal to K_u; K is the torque constant of the motor; and u is the representative controlled quantity. Thus, (16) can be rewritten as (24).

$$\begin{aligned} &J_T\ddot{\theta_m} + \frac{D_p}{2\pi\eta D_m} J_m \theta \\ &\quad = Ku - D\omega - \frac{D_p}{2\pi\eta D_m} T_{friction} - \frac{D_p}{2\pi\eta D_m} T_L \end{aligned} \tag{24}$$

According to the characteristic of the hydraulic system described by (25), (24) is equal to (26).

$$\theta = \frac{D_p}{2\pi D_m}\ddot{\theta_m} \tag{25}$$

$$(J_T + \frac{D_p}{2\pi\eta D_m}J_m\frac{D_p}{2\pi D_m})\ddot{\theta_m} = Ku - D\omega - \frac{D_p}{2\pi\eta D_m}T_{friction} - \frac{D_p}{2\pi\eta D_m}T_L \tag{26}$$

$$J_1\ddot{\theta_m} = Ku - D\omega - M_f - T_r \tag{27}$$

In (27),$J_1 = J_T + \frac{{D_p}^2}{4\pi^2\eta D_m}J_m\frac{1}{D_m}$, $M_f = \frac{D_p}{2\pi\eta D_m}T_{friction}$, $T_r = \frac{D_p}{2\pi\eta D_m}T_L$.

The friction torque is described by (17)−(23); hence, M_f can be described by (28).

$$M_f = \frac{D_p}{2\pi\eta D_m}[\alpha_f(\sigma_{01}z + \sigma_{11}\frac{dz}{dt}) + \sigma_{21}v] = \alpha_f(\sigma_0 z + \sigma_1\frac{dz}{dt}) + \sigma_2 v \tag{28}$$

In (28), $\sigma_0 = \frac{D_p}{2\pi\eta D_m}\sigma_{01}$, $\sigma_1 = \frac{D_p}{2\pi\eta D_m}\sigma_{11}$, $\sigma_2 = \frac{D_p}{2\pi\eta D_m}\sigma_{21}$, and α_f is the coefficient that describes the transform of the friction force and is equal to one in the normal state.

Hence,

$$J_1\ddot{\theta_m} = Ku - D\omega - \alpha_f(\sigma_0 z + \sigma_1\frac{dz}{dt}) + \sigma_2 v - T_r \tag{29}$$

Because $v = Dp\omega/2\pi D_m$, (29) can be rewritten as (30).

$$J_1\ddot{\theta_m} = Ku - D\omega - \alpha_f(\sigma_0 z + \sigma_1\frac{dz}{dt}) + \sigma_2 K_v\omega - T_r \tag{30}$$

Using the system function above and the integral back-stepping adaptive strategy, the self-adaption controller is designed based on the steady theory aimed to describe the nonlinear friction by the recursive Lyapunov function, making the system output accurately approximate the virtual desired trajectory. This realizes the system ability of stabilization and self-adaption. Assuming the system states $\theta(t)$ are reasonable, the above assumption can be achieved in a practical control process. Fig. 4 shows the control schemes of the integral back-stepping adaptive strategy.

Step 1: Define the angle-trace error signal e_1, as in (31).

$$e_1 = \theta_d - \theta \tag{31}$$

Therefore, its error dynamics equation is (32).

$$\dot{e} = \dot{\theta_d} - \dot{\theta} = \dot{\theta_d} - \omega \tag{32}$$

In (32), ω is the virtual input. Using the integral back-stepping control algorithm, according to the stability theory, we recursively determine the value of expectation of ω via the input error signal e_1. Therefore, selecting the controlling Lyapunov function V_1 as (34), the derivation result is given by (34).

$$V_1 = \frac{1}{2}e_1^2 \tag{33}$$

$$\dot{V_1} = e_1\dot{e_1} = -k_1e_1^2 + e_1(k_1e_1 + \dot{\theta_d} - \omega) \tag{34}$$

Establishing the value of expectation of ω as ω_d, $V_1 \le 0$, and ω_d are given by (35) to ensure that the system remains stable.

$$\omega_d = k_1e_1 + k\theta + \dot{\theta_d} \tag{35}$$

$\theta = \int_0^t e_1(\tau)d\tau$ is the effective angle-trace error integral, which ensures that in the condition of load disturbance and model uncertainty, the tracking error is approximately zero. k_1 and k are positive and can be designed.

Step 2: The angular velocity ω is not the actual controlled variable; hence, error e_2 exists between the angular velocity ω and its desired value ω_d, which can be expressed as (36).

$$e_2 = \omega_d - \omega = k_1e_1 + k\theta + \dot{\theta_d} - \omega \tag{36}$$

Based on (32) and (26), e_1 can also be expressed as (37).

$$\dot{e_1} = e_2 - k_1e_1 - k\theta \tag{37}$$

Thus, e_2 is expressed as (38).

$$\dot{e_2} = k_1\dot{e_1} + k_1e_1 + \dot{\theta_d} - \dot{\omega} \tag{38}$$

We can obtain (39) based on (29) and (30).

$$\begin{aligned} J_1\dot{e_2} &= J_1k_1\dot{e_1} + J_1k_1e_1 + J_1\ddot{\theta_d} - Ku + D\omega \\ &\quad + \theta(\sigma_0 z + \sigma_1\frac{dz}{dt}) + \sigma_2k_v\omega + T_r \\ &= J_1k_1\dot{e_1} + J_1k_1e_1 + J_1\ddot{\theta_d} - Ku + D\omega + \theta\sigma_0 z \\ &\quad + \theta\sigma_1k_v\omega - \sigma_1k_v\frac{|\omega|}{g(\omega)}z + \sigma_2k_v\omega + T_r \end{aligned} \tag{39}$$

J, θ, D, and T_r are uncertain parameters. The actual values are not available; thus, $\hat{J}$, $\hat{\theta}$, $\hat{D}$, and T_r must be rounded off as actual values. We then choose (40) as the control strategy.

$$\begin{aligned} Ku &= \hat{J}_1(k_1\dot{e}_1 + k_1e_1\ddot{\theta_d}) + e_1 + k_ce_2 + \hat{D}\omega \\ &\quad + \hat{\theta}\sigma_1k_v\omega - \hat{\theta}\sigma_1k_v\omega\frac{|\omega|}{g(\omega)}\hat{z} + k_v\hat{\sigma_2} + \hat{T_r} \end{aligned} \tag{40}$$

In (40), the design constant k_v>0; thus, (39) can be rewritten as (41).

$$\begin{aligned} J_1\dot{e_2} &= \widetilde{J_1}(k_1\dot{e_1} + k_1e_1\ddot{\theta_d}) - (e_1 + k_ce_2) + \widetilde{D}\omega(\theta\sigma_0 z - \hat{\theta}\sigma_0\hat{z}) \\ &\quad + \widetilde{\theta}\sigma_1k_v\omega + (\hat{\theta}\sigma_1k_v\omega\frac{|\omega|}{g(\omega)}z - \theta\sigma_1k_v\frac{|\omega|}{g(\omega)}z) \\ &\quad + k_v\widetilde{\sigma_2}\omega + \widetilde{T_v} \end{aligned} \tag{41}$$

$\theta z - \hat{\theta}\hat{z} = \theta\tilde{z} + \tilde{\theta}\tilde{z}$; therefore, $\dot{e_2}$ can be expressed as (42).

$$\begin{aligned} J_1\dot{e_2} &= \frac{\widetilde{J_1}}{J_1}(k_1\dot{e}_1 + k_1e_1\ddot{\theta_d}) + \frac{1}{J_1}[\widetilde{D}\omega + \widetilde{\sigma_2}k_v\omega + \widetilde{T_v} - e_1 \\ &\quad - k_ce_1 + \widetilde{\theta}\sigma_1k_v\omega + (\sigma_0 - \sigma_1k_v\frac{|\omega|}{g(\omega)})(\theta\widetilde{z} + \widetilde{\theta}\hat{z})] \end{aligned} \tag{42}$$

Select the positive definition of the Lyapunov function as (43).

$$\begin{aligned} V &= \frac{1}{2}{e_1}^2 + \frac{1}{2}J_1{e_2}^2 + \frac{1}{2}k\chi^2 + \frac{1}{2}\theta\widetilde{z^2} + \frac{1}{2r_1}\widetilde{\sigma_2^2} + \frac{1}{2r_0}\widetilde{\theta^2} \\ &\quad + \frac{1}{2r_2}\widetilde{T_v^2} + \frac{1}{2r_3}\widetilde{D^2} + \frac{1}{2r_4}\widetilde{J_1^2} \end{aligned} \tag{43}$$

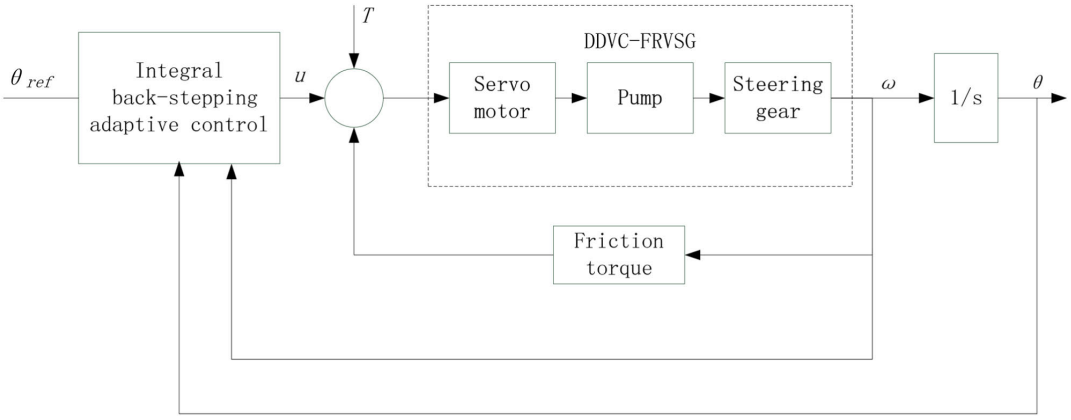

FIGURE 4. Control schemes of the integral back-stepping adaptive strategy.

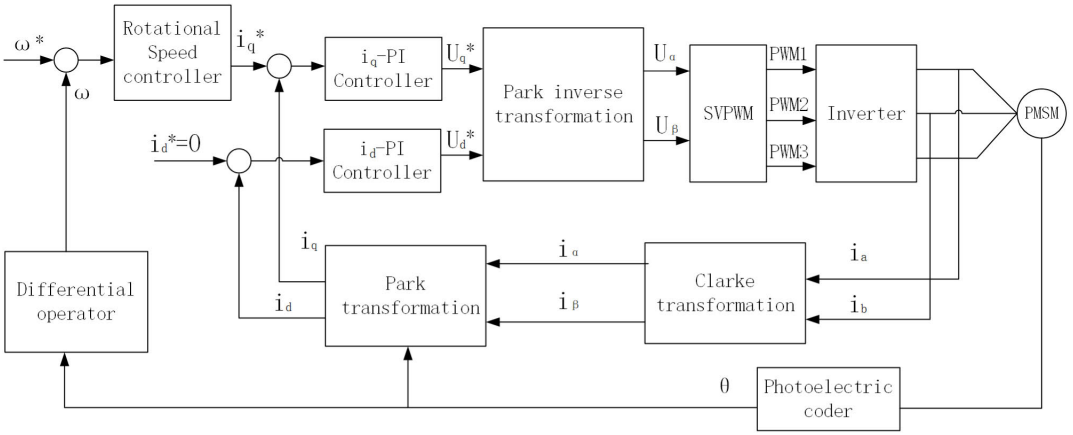

FIGURE 5. Structure of AC PMSM control system.

In (43), r_n (n=0,1.2.3) is the adaptive gain. Moreover, after rearranging the equation for V, we obtain (44).

$$\begin{aligned}\dot{V} &= -k_c {e_1}^2 - \theta k_v \frac{|\omega|}{g(\omega)}\tilde{z}^2 \\ &\quad -J_1(-e_2 k_1 \dot{e_1} - e_2 k_1 e_1 - e_2 \ddot{\theta}_d + \frac{1}{r_4}\dot{\hat{J}}_1) \\ &\quad -\tilde{D}(e_2\omega + \frac{1}{r_3}\dot{\hat{D}}) \\ &= -\dot{\hat{T}}_v(-e_2 + \frac{1}{r_2}\dot{\hat{J}}_1) - \tilde{\sigma_2}(-e_2 k_v \omega + \frac{1}{r_1}\dot{\hat{\sigma_2}}) + \tilde{\theta} \\ &\quad -(e_2\hat{z}\sigma_0 - e_2\hat{z}\sigma_1\omega\frac{|\omega|}{g(\omega)} - \frac{1}{r_0}\dot{\hat{\theta}} + e_2 k_v \sigma_1 \omega \qquad (44)\end{aligned}$$

If we choose (45) as the adaptive strategy, it could lead to (46).

$$\dot{\hat{\theta}} = r_0(e_2\ddot{\theta}_d - e_2\hat{z}\sigma_1 k_v \frac{|\omega|}{g(\omega)} + e_2 k_v \sigma_1 \omega) \qquad (45)$$

$$\dot{V} = -k_c {e_2}^2 - k_1 {e_1}^2 - \theta k_v \frac{|\omega|}{g(\omega)}\tilde{z}^2 \qquad (46)$$

k_1>0, k_c>0, $\frac{|\omega|}{g(\omega)}$>0, k_v>0, θ>0; thus, $\dot{V} \leq 0$.

According to the Lyapunov stability theory, the control system can steadily track the expected trajectory. Thus,

$$\lim_{t\to+\infty} |\theta_d - \theta| = 0$$

and the output error

$$\lim_{t\to+\infty} |e_1| = \lim_{t\to+\infty} |\theta_d - \theta| = 0$$

V. SIMULATION STUDY

A. MOTOR CONTROL SCHEME

The AC PMSM referred to in this paper adopts a double closed-loop control system (revolving speed and current), with the control system structure shown in Fig. 5.

B. THE SIMULATION MODEL

The simulation model is estimated based on the united simulation of AMEsim/Simulink. The simulation model is divided into two types to compare the effect before and after compensation:

1) Simulation model only with the normal PID control strategy.

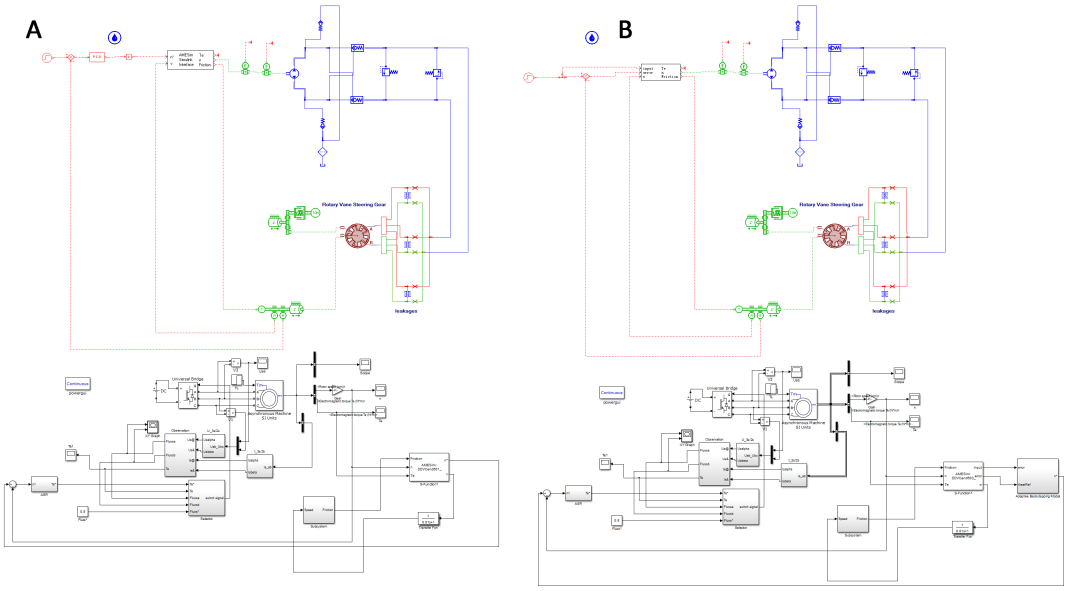

FIGURE 6. Simulation model: (A) simulation model without compensation. (B) simulation model with integral back-stepping adaptive method.

2) Simulation model compensated with the integral back-stepping adaptive control strategy.

Fig. 6 shows the two types of simulation model.

In the model, the main component used consists of an AC motor, a motor drive, a coupling, a gear pump, a pre-pressing oil tank, an oil support device, a rotary vane steering gear, a rudder blade, a feedback device, and an AMEsim-Simulink interface module. In the simulation, the AC motor uses the vector control method for control.

The AC motor was rotated in the Simulink platform when the simulation started. The rotary speed and the torque were transmitted through the AMEsim–Simulink interface module to the AMEsim model. It drove the gear pump, and the pump in turn rotated the vane cylinder. The cylinder rotated the rudder blade. The parameters of the rudder angle were collected via the rudder angle sensor feedback through the AMEsim–Simulink interface module to the Simulink platform. The output power of the motor was collected via a power sensor.

VI. RESULTS

Figs. 7−9 shows the test results of the rotary vane steering gear under non-compensation control and integral back-stepping adaptive control. In Figs. 7−9, subgraph A represents the degree response, Subgraph B represents the power response, subgraph C represents one phase of the three-phase current, and subgraph D represents one phase of the two-phase rotating coordinate voltage.

A. DYNAMIC RESPONSE

Fig. 7 shows the steering gear driven via a positive step signal. During startup, when the value of the output torque from the rotary vane cylinder to the rudder blade (output) is less than the value of the maximum static friction torque, the rudder blade begins to exhibit a starting dead zone, such as the short-dashed line shown from 0.2 s to 0.26 s that continues for 0.06 s, as shown in Fig. 7A. Repeating the mutual conversion between dynamic friction and static friction at a low speed, the rudder blade begins to exhibit a stick-slip phenomenon, as shown by the short-dashed line from 0.26 s to 0.37 s in Fig. 7A. With the rudder blade rotary vane at normal speed, tracking with the control order imposed on the servomotor drives the hydraulic system operation (the short-dashed line shown from 0.37 s to 0.57 s in Fig. 7A). When approaching the input signal, the stick-slip phenomenon then occurred with a smaller amplitude and lasted for 0.38 s (the short-dashed line shown from 0.57 s to 0.95 s in Fig. 7A). The starting dead zone phenomenon present in the adaptive back-stepping state considerably decreased. The dead zone from 0.2 s to 0.207 s (i.e., the long-dashed line in Fig. 7A), which continued for 0.007 s, considerably shortened compared to the dead zone of 0.05 s (the short-dashed line shown from 0.2 s to 0.25 s in Fig. 7A). The stick-slip phenomenon was almost eliminated via compensation by the integral back-stepping adaptive method (in the long-dashed line shown in Fig. 7A).

Fig. 8 shows the steering gear driving by a negative step signal. During the startup, a starting dead-zone area exists (the short-dashed line shown from 0.2 s to 0.43 s, continuing to 0.23 s in Fig. 8A). Like the long-dashed line shown in Fig. 8A, the dead zone from 0.2 s to 0.217 s and continues for 0.017 s. Moreover, compared to 0.23 s of the short-dashed line shown from 0.2 s to 0.43 s in Fig. 8A, further substantial reduction is achieved. Repeating the mutual conversion between dynamic friction and static friction at a low speed, as in Fig. 8A, the rudder blade exhibits the stick-slip phenomenon (the short-dashed line from 0.57 s to 46 s in Fig. 8A), which

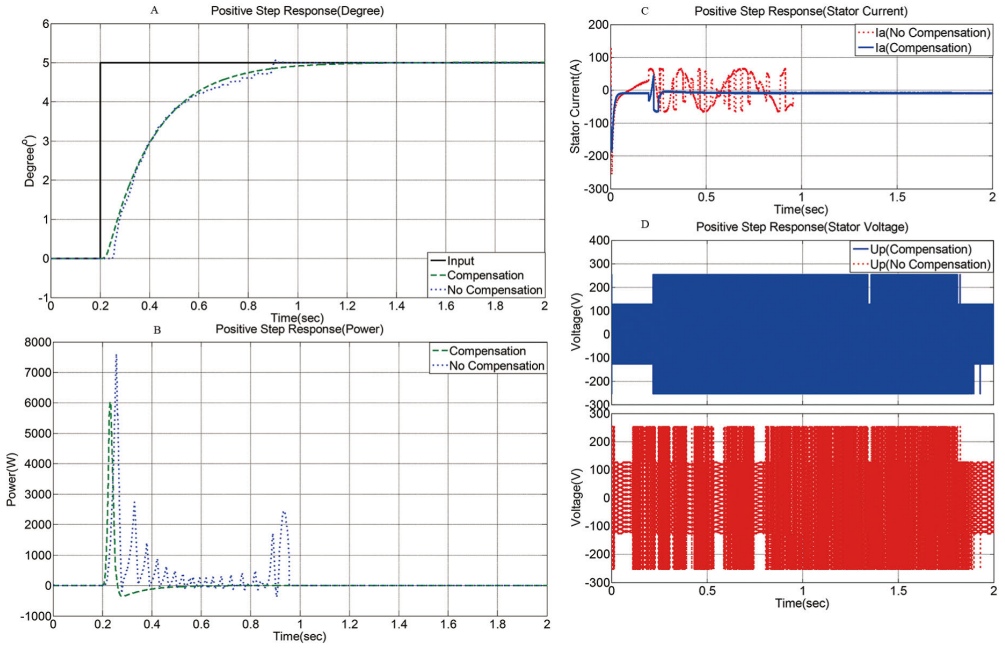

FIGURE 7. Positive step response: (A) dynamic response (degree). (B) energy consumption (power).

was almost eliminated in the long-dashed line of Fig. 8A via compensation by the integral back-stepping adaptive method.

Fig. 9 shows the steering gear driven by a sinewave signal. In the startup, a starting dead zone can also be observed (the short-dashed line shown from 0 s to 0.007 s in Fig. 9A). When the direction of the input order is changed, the rotary speed of the rudder blade gradually decreases and approaches zero speed from the positive direction. Therefore, the rotary speed of the rudder blade approaches the low-velocity state. The instantaneous speed is zero when the rudder achieves its vertex point. The rotary direction then changes and returns to the process of starting, which overcomes the static friction torque. Therefore, the flat-topped phenomenon is exhibited during almost the entire process of changing direction. The stick-slip phenomenon then occurred with a obviously amplitude and lasted for almost all of the negative process (the short-dashed line shown from 1.128 s to 3.778 s , and 6.128 s to 8.778 s in Fig. 9A). From the long-dashed line shown in Fig. 9A, the duration of the stick-slip phenomenon, which is present in the no-compensation state, has been compensated by the integral back-stepping adaptive method and has almost been eliminated in the process of negative direction (the long-dashed line shown in Fig. 9A).

B. ENERGY CONSUMPTION

Fig. 7B shows the response of power that the steering gear has driven via a positive step signal. To operate with the input order, the steering gear without compensation must increase the power to overcome the starting dead zone. Therefore, the maximum output power of the motor was 7.62 kW (the short-dashed line shown from 0.2 s to 0.26 s in Fig. 7B). The steering gear increased the power to change the static friction to dynamic and overcome the stick-slip phenomenon. Therefore, like the short-dashed line shown from 0.26 s to 0.37 s in Fig. 7B and corresponding to each stick-slip phenomenon in Fig. 7A, a significant power increase was observed. According to the short-dashed line shown from 0.37 s to 0.57 s in Fig. 7B and corresponding to the normal speed operating range, the envelope curve of power shows a smooth downward trend. However, corresponding to the stick-slip phenomenon that occurred with a smaller amplitude range (the short-dashed line shown from 0.57 s to 0.95 s in Fig. 7B), it leveled off after 0.97 s after a slight upward trend of the envelope curve. In the compensation state, under the action of the compensation strategy, the dead zone only continued for 0.007 s. The stick-slip phenomenon was almost eliminated via compensation by the integral back-stepping adaptive method; therefore, after overcoming the transient dead zone, the steering gear directly operated at normal speed, such that the maximum output power of the motor reached only 6.02 kW (the long-dashed line shown from 0.2 s to 0.207 s in Fig. 7B). The envelope curve of power rapidly showed a smooth downward trend (the long-dashed line shown from 0.217 s to 0.57 s in Fig. 7B). After 0.57 s, the envelope curve of power tended to zero.

Fig. 8B shows the response of power that the steering gear drove via a negative step signal. The maximum output power of the motor for overcoming the starting dead zone was 16 kW (the short-dashed line shown from 0.2 s to 0.43 s in Fig. 8B). The steering gear increased the power to change the static friction to dynamic and overcome the stick-slip phenomenon. Therefore, like the short-dashed line shown from

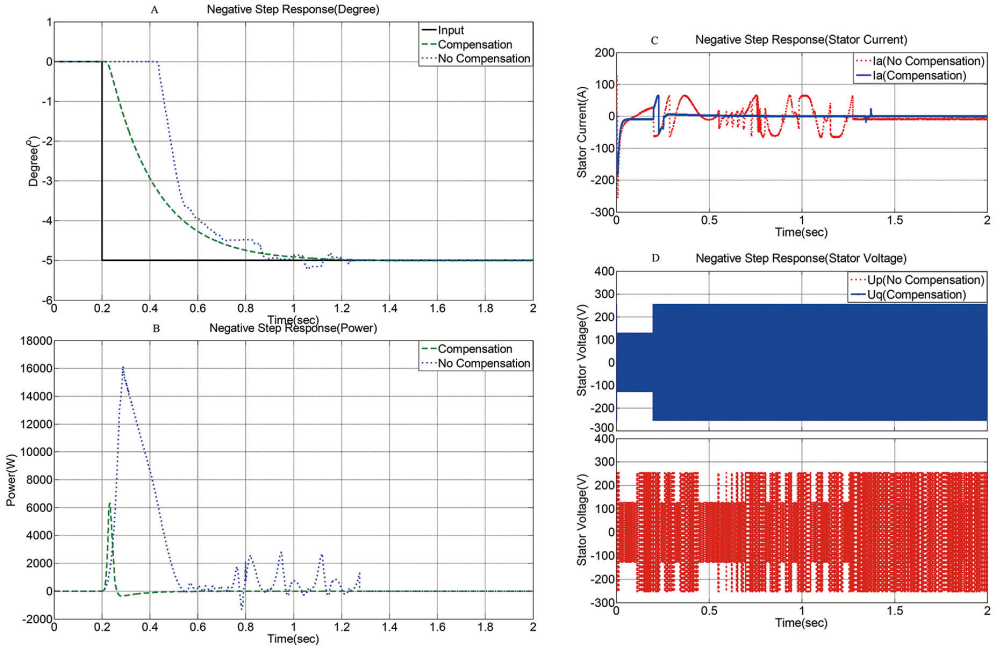

FIGURE 8. Negative step response: (A) dynamic response (degree). (B) energy consumption (power).

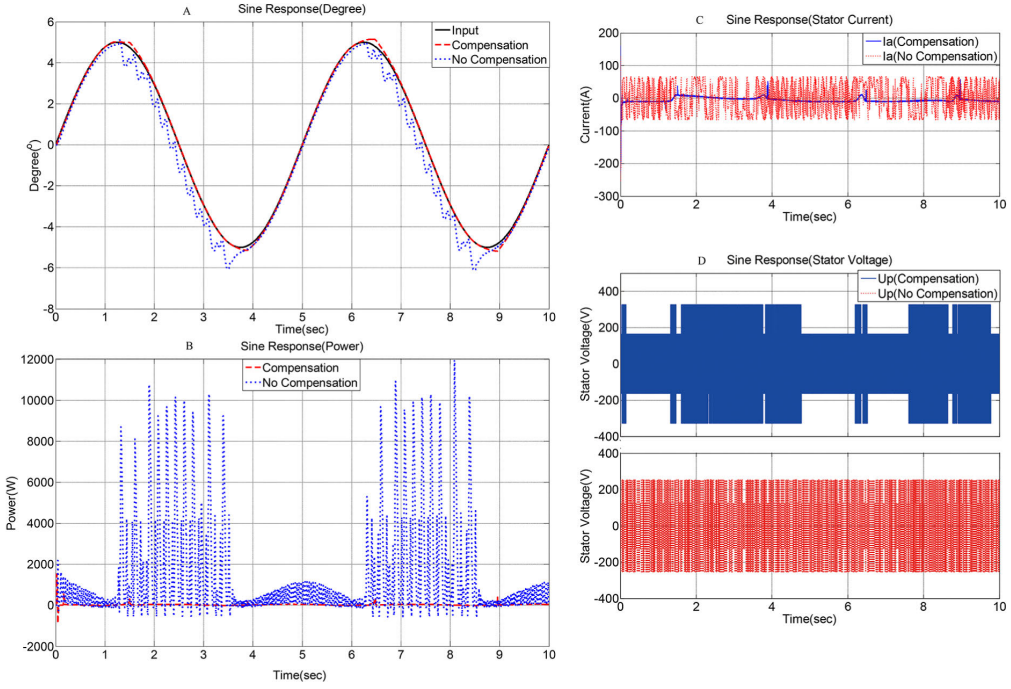

FIGURE 9. Sine wave response: (A) dynamic response (degree). (B) energy consumption (power).

0.57 s to 1.23 s in Fig. 8B and corresponding to each stick-slip phenomenon in Fig. 8A, a significant power increase was observed. Like the short-dashed line shown in Fig. 8B, the envelope curve of power showed a smooth downward trend, and no obvious upward trend was observed. In the compensation state, under the action of the compensation strategy, the dead zone only continued for 0.017 s. The stick-slip phenomenon was almost eliminated via compensation by the integral back-stepping adaptive method; therefore, after overcoming the transient dead zone, the steering gear directly operated as normal speed, such that the maximum output power of the motor reached only 6.2 kW (the long-dashed

line shown from 0.2 s to 0.217 s in Fig. 8B). The envelope curve of power rapidly shows a smooth downward trend (the long-dashed line shown from 0.217 s to 1.213 s in Fig. 8B). After 1.213 s, the envelope curve of power tended to be zero.

Fig. 9B presents the response of power that the steering gear drove via a sine wave signal. In the startup, a starting dead zone was observed (the short-dashed line shown from 0 s to 0.33 s in Fig. 9B). Both flat-topped and stick-slip phenomena occurred when the direction of the input order changed. Like Figs. 7B and 8B, corresponding to each dead zone, the flat-topped and stick-slip, the steering gear increased the power to overcome the nonlinear phenomenon. The maximum of the output power of the motor was 11.89 kW. As shown by the long-dashed line in Fig. 9B, the nonlinear phenomenon present in the no-compensation state was compensated by the integral back-stepping adaptive method and was almost eliminated. Accordingly, the curve changed more smoothly. Therefore, the output power of the motor was greatly reduced, especially corresponding to the various nonlinear phenomena in Fig. 9A (the long-dashed line shown in Fig. 9A).

VII. CONCLUSION

In this study, concepts of electro-hydraulic engineering and compensation methods were combined to design a controller to contribute to the energy-saving performance and efficient energy requirement for the DDVC–FRVSG system. We proposed an integral back-stepping adaptive method to suppress nonlinear rudder friction and effectively and precisely control the system. As a result, the loss of power caused by the friction torque was greatly reduced. We conducted a rudder degree response simulation and motor power response simulation for the DDVC–FRVSG under two states: noncompensation control and integral back-stepping adaptive control. The study makes a significant contribution to the literature because integral back-stepping adaptive strategy showed a better performance. In terms of the dynamic response, compared to the no-compensation state, integral back-stepping adaptive method improved by 73.08% on average. In terms of energy saving, compared to the no-compensation state, integral back-stepping adaptive method improved by 36.39 % on average. Therefore, the adaptive back-stepping compensation method not only effectively suppressed the nonlinear friction torque and ensured a stable DDVC–FRVSG operation but also effectively reduced the output power of the driving motor and ensured the high-efficiency operation of DDVC–FRVSG with low energy consumption.

In the actual operating environment of the steering gear, the influence of the unfiltered interference on the dynamic performance of the steering system and the system power consumption must still be considered. In the process of suppressing the external interference and nonlinear friction through the control strategy, regardless of whether the control strategy proposed herein can achieve the same effect in a physical test, a test platform must be designed and verified through a prototype test. The compensation control strategy proposed herein was based on a friction model. If the compensation method was not based on the friction model, the compensation effect for the dynamic performance and the energy-saving effect of the output power will be compared with the method proposed herein. The better performance must be verified by comparative tests.

Our future work will involve the design of a test bench according to the test tank to simulate the external disturbances experienced by the DDVC–FRVSG in a real marine environment. Compensating the steering by integral back-stepping adaptive method, we will compare the results with those of the no-compensation state, as in this study. The difference between the test results and the simulation results will also be verified by a prototype test. Our future work will also involve the proposal of a compensation method that is not based on the friction model for DDVC–FRVSG. We aim for the dynamic performance and energy-saving effect of the output power and compare the effect with the methods proposed herein.

ACKNOWLEDGMENT

The authors would like to thank Editage [www.editage.cn] for English language editing.

Compliance with ethical standards.

Conflict of interest. The authors declare that they have no conflict of interest concerning the publication of this manuscript.

REFERENCES

[1] M. D. A. Al-Falahi, T. Tarasiuk, S. G. Jayasinghe, Z. Jin, H. Enshaei, and J. M. Guerrero, "AC ship microgrids: Control and power management optimization ," *Energies*, vol. 11, no. 6, p. 1458, 2018.

[2] P. T. Deng, "Dynamic characteristics analysis and study of high-speed high-frequency marine steering gear," *Ship Eng.*, vol. 5, pp. 40–44, May 2015.

[3] A. Witkowska, M. Tomera, and R. Mierzchalski, "A backstepping approach to ship course control," *Int. J. Appl. Math. Comput. Sci.*, vol. 17, no. 1, pp. 73–85, Mar. 2007.

[4] J. van Amerongen, P. G. M. van der Klugt, and H. R. van Nauta Lemke, "Rudder roll stabilization for ships," *Automatica*, vol. 26, no. 4, pp. 679–690, Jul. 1990.

[5] W. H. Su and J. H. Jiang, "Parameter identification of direct drive electro-hydraulic servo rotary vane steering gear based on genetic ant colony algorithm," *J. Harbin Inst. Technol.*, vol. 42, no. 11, pp. 1730–1733, Nov. 2010.

[6] T. Zhen, L. Yingying, and H. Song, "Study of identification for nonlinear system of electronic actuator," *Comput. Meas. Control*, vol. 24, no. 5, pp. 110–112, May 2016.

[7] M. Ito, "DDVC (direct drive volume control) oil-hydraulic actuator and its some applications," *IEEE/ASME Trans. Mechatronics*, vol. 43, pp. 295–302, Aug. 2015.

[8] H. Yanada and H. Ohnishi, "Frequency-shaped sliding mode control of an electrohydraulic servo-motor," *Proc. Inst. Mech. Eng., I, J. Syst. Control Eng.*, vol. 213, no. 6, pp. 441–448, Sep. 1999.

[9] H. Yanada, T. Matsuo, and N. Matsumoto, "Application of model reference frequency-shaped sliding mode control with pre-filter to an electrohydraulic servo motor," in *Proc. Int. Microprocesses Nanotechnol. Conf.*, Sep. 2003, pp. 19–26.

[10] M. Y. Zhang, H. B. Yang, J. B. Zhang, T. C. Ding, and H. G. Jia, "Servo system of harmonic drive electromechanical actuator using improved ADRC," *Proc. Inst. Mech. Eng., I, J. Syst. Control Eng.*, vol. 22, no. 1, pp. 99–108, Jan. 2014.

[11] R. Wang, Z. Mei, X. Li, and J. Wang, "Research on adaptive nonlinear friction compensation of mechatronic servo systems," *Proc. Chin. Soc. Elect. Eng.*, vol. 32, no. 36, pp. 123–129, Dec. 2012.

[12] X. Xingzhi, G. Yakui, and Z. Weiguo, "Analyzing structural nonlinear flutter characteristics for a rudder with dynamic stiffness considered," *J. Northwestern Polytechnical Univ.*, vol. 33, no. 3, p. 20, Mar. 2015.
[13] F. Heidtmann and M. Bröcker, "Nonlinear modeling and tracking control of a hydraulic rotary vane actuator," *Proc. Appl. Math. Mech.*, vol. 5, no. 1, pp. 161–162, Jan. 2010.
[14] M. T. S. Aung and R. Kikuuwe, "Stability enhancement of admittance control with acceleration feedback and friction compensation," *Mechatronics*, vol. 45, pp. 110–118, Aug. 2017.
[15] L. P. Wang, "Optimal sliding mode control for a class of affine nonlinear systems with uncertainties," M.S. thesis, Qingdao Univ. Sci. Technol., Qingdao, China, Jun. 2010, pp. 19–23.
[16] C. Jin, *On Problem of the Deeentralized Model Reference Adaptive Control for the Large Scale Systems*. Boston, MA, USA: Northeastern Univ., Jun. 2009, pp. 8–14.
[17] Q. J. Xiao, "Study on multiple sliding mode control and nonlinear compensation for EMA with harmonic gear drive," Ph.D. dissertation, Changchun Inst. Opt., Changchun, China, Jun. 2013, pp. 3–7.
[18] X. D. Wang, "Friction and its compensation method in load simulator," *China Mech. Eng.*, vol. 14, no. 6, pp. 511–514, Mar. 2003.
[19] R. Scattolini, C. Siviero, M. Mazzucco, S. Ricci, L. Poggio, and C. Rossi, "Modeling and identification of an electromechanical internal combustion engine throttle body," *Control Eng. Pract.*, vol. 5, no. 9, pp. 1253–1259, Sep. 1997.
[20] A. Yazdizadelh and K. Khorasani, "Adaptive friction compensation based on the Lyapunov scheme," in *Proc. IEEE Int. Conf. Control Appl.*, Sep. 1996, pp. 1060–1065.
[21] C. C. de Wit, "Robust control for servo-mechanisms under inexact friction compensation," *Automatica*, vol. 29, no. 3, pp. 757–761, May 1993.
[22] D. P. Hess and A. Soom, "Friction at a lubricated line contact operating at oscillating sliding velocities," *J. Tribol.*, vol. 112, no. 1, pp. 147–152, Jan. 1990.
[23] A. Kebairi, M. Becherif, and M. E. Bagdouri, "Modelling, simulation and identification of an engine air path electromechanical actuator," *Control Eng. Pract.*, vol. 34, pp. 88–97, Jan. 2015.
[24] L. Le-Tien and A. Albu-Schäffer, "Robust adaptive tracking control based on state feedback controller with integrator terms for elastic joint robots with uncertain parameters," *IEEE Trans. Control Syst. Technol.*, vol. 26, no. 6, pp. 2259–2267, Nov. 2018.
[25] Y. Pan, H. Wang, X. Li, and H. Yu, "Adaptive command-filtered backstepping control of robot arms with compliant actuators," *IEEE Trans. Control Syst. Technol.*, vol. 26, no. 3, pp. 1149–1156, Mar. 2018.
[26] S. E. Lyshevski, "Control of high-precision direct-drive mechatronic servos: Tracking control with adaptive friction estimation and compensation," *Mechatronics*, vol. 43, pp. 1–5, May 2017.
[27] N. Liu, X. Shao, and W. Yang, "Integral barrier Lyapunov function based saturated dynamic surface control for vision-based quadrotors via backstepping," *IEEE Access*, vol. 6, pp. 63292–63304, 2018.
[28] K. A. J. Verbert, R. Tóth, and R. Babuška, "Adaptive friction compensation: A globally stable approach," *IEEE/ASME Trans. Mechatronics*, vol. 21, no. 1, pp. 351–363, Feb. 2016.
[29] J. Yao, W. Deng, and W. Sun, "Precision motion control for electro-hydraulic servo systems with noise alleviation: A desired compensation adaptive approach," *IEEE/ASME Trans. Mechatronics*, vol. 22, no. 4, pp. 1859–1868, Aug. 2017.
[30] R. Kelly, V. Santiban, and E. Gonzalez, "Adaptive friction compensation in mechanisms using the Dahl model," *Proc. Inst. Mech. Eng., I, J. Syst. Control Eng.*, vol. 218, no. 1, pp. 53–57, Feb. 2004.
[31] Y. Tan, J. Chang, and H. Tan, "Adaptive backstepping control and friction compensation for AC servo with inertia and load uncertainties," *IEEE Trans. Ind. Electron.*, vol. 50, no. 5, pp. 944–952, Oct. 2003.
[32] W. F. Xie, "Sliding-mode-observer-based adaptive control for servo actuator with friction," *IEEE Trans. Ind. Electron.*, vol. 54, no. 3, pp. 1517–1527, Jun. 2007.
[33] C. C. de Wit and P. Lischinsky, "Adaptive friction compensation with partially known dynamic friction mode," *Int. J. Adapt. Control Signal Process.*, vol. 11, no. 1, pp. 65–80, Feb. 1997.
[34] F. Altpeter, "Friction modeling, identification and compensation," M.S. thesis, EPFLPPUR, Jun.1999, pp. 73–89.
[35] B. Borsotto, E. Godoy, D. Beauvois, and E. Devaud, "An identification method for static and coulomb friction coefficients," *Int. J. Control, Automat. Syst.*, vol. 7, no. 2, pp. 305–310, Apr. 2009.
[36] V. Lampaert, F. Al-Bender, and J. Swevers, "Experimental characterization of dry friction at low velocities on a developed tribometer setup for macroscopic measurements," *Tribology Lett.*, vol. 16, nos. 1–2, pp. 95–105, Feb. 2004.
[37] Y. D. Chen, X. S. Qin, M. J. Jiang, and S. Q. Zhang, "Key technologies in the friction text of actuator drive system," *Meas. Control Technol.*, vol. 28, no. 7, pp. 88–90, Jul. 2009.
[38] S.-J. Huang and C.-M. Chiu, "Optimal LuGre friction model identification based on genetic algorithm and sliding mode control of a piezoelectric-actuating table," *Trans. Inst. Meas. Control*, vol. 31, no. 2, pp. 181–203, Apr. 2009.
[39] Y. L. Ma, J. Huang, and D. Zhang, "Backlash compensation in servo systems based on adaptive Backstepping-control," *Control Theory Appl.*, vol. 25, no. 6, pp. 1090–1094, Jun. 2008.
[40] D. Zang, *Compensation Control of Servo Systems With Friction*. Xi'an, China: Xidian Univ., Jun. 2008, pp. 27–36.
[41] Y. L. Ma, J. Huang, and D. Zhang, "Adaptive compensation of backlash nonlinearity for servo systems," *J. Syst. Simul.*, vol. 21, no. 5, pp. 1498–1501, May 2009.
[42] J. Zhou, J. Huang, P. Li, and N. Li, "Hybrid modeling of microwave devices using multi-kernel support vector regression with prior knowledge," *Int. J. RF Microw. Comput.-Aided Eng.*, vol. 25, no. 3, pp. 219–228, May 2014.
[43] J. Zhou, J. Huang, L. Song, D. Zhang, and Y. Ma, "Electromechanical co-design and experiment of structurally integrated antenna," *Smart Mater. Struct.*, vol. 24, no. 3, Feb. 2015, Art. no. 037004.
[44] L. Liang, L. Wang, and J. Wang, "The compensation for nonlinear friction of DDVC flange-type rotary vane steering gear," *PLOS ONE*, vol. 13 no. 11, Nov. 2018, Art. no. e0207018.

L. H. LIANG received the Ph.D. degree in control science and engineering from Harbin Engineering University, Harbin, China, in 2003.

In 1995, he joined Harbin Engineering University. In 2002, he joined the Ship Stabilization and Control Research Unit, College of Automation, Harbin Engineering University, as an Associate Professor, where he has been a Professor, since 2005. His current research interests include ship stabilization control, ship attitude control, and electro-hydraulic servo systems.

L. Y. WANG received the B.S. degree in electronic and information engineering from the Harbin University of Commerce, Harbin, China, in 2010, and the M.S. degree in control science and engineering from Harbin Engineering University, Harbin, in 2014, where he is currently pursuing the Ph.D. degree in control science and engineering.

J. F. WANG was born in Bengbu, Anhui, China, in 1978. He received the B.S., M.S., and Ph.D. degrees in mechanical engineering from the Harbin Institute of Technology, Harbin, China, in 2006.

In 2006, he joined the Ship Stabilization and Control Research Unit, College of Automation, Harbin Engineering University, as a Lecturer, where he has been an Associate Professor, since 2009. His current research interests include ship attitude control and electro-hydraulic servo systems.